

# 6

## Thermodynamics–Structure Correlations of Sulfonamide Inhibitor Binding to Carbonic Anhydrase

Daumantas Matulis and Matthew Todd

### 6.1 Introduction

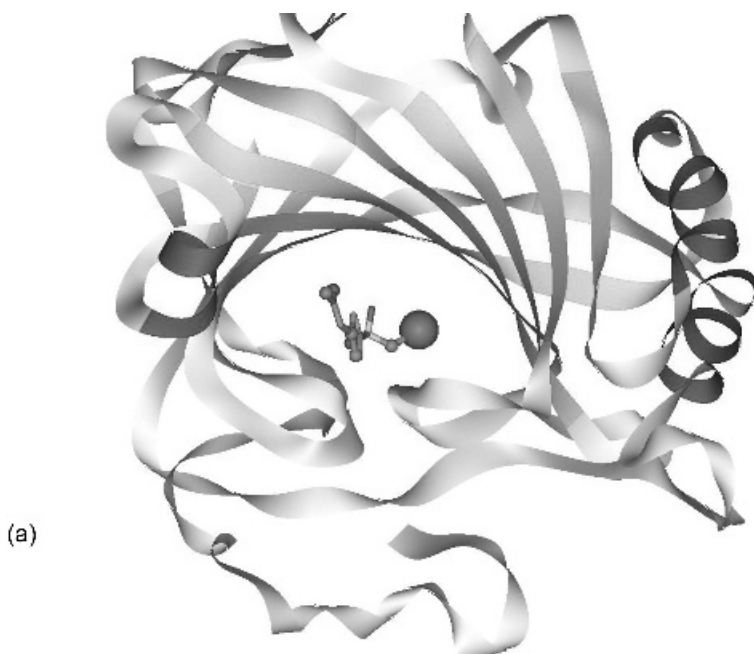
Microcalorimetry is an excellent method of determining the thermodynamics of ligand–protein binding in solution, because the signal being measured is the observed binding enthalpy ( $\Delta_{\text{b-obs}}H$  [Editors' note: this term can also be written  $\Delta H_{\text{obs}}$  or  $\Delta_{\text{b}}H_{\text{obs}}$  as seen elsewhere in this book]), which is free of any model assumptions. The affinity ( $\Delta_{\text{b}}G$ ) can be computed from the shape of a binding curve, and the binding entropy ( $\Delta_{\text{b}}S$ ) is obtained from the difference between the two. The calorimetrically observed binding enthalpy, however, can be the sum of several partial reactions, including changes in the protonation of ligand, protein, and buffer, each of which may have its own contribution to the observed enthalpy of binding. Which enthalpy is the 'true' enthalpy of a reaction? In order to obtain an enthalpy of binding that can be correlated with structure, one must elucidate the thermodynamics for all reactions that occur simultaneously upon ligand binding. It is fairly straightforward to distinguish net protonation effects by measuring  $\Delta_{\text{b-obs}}H$  in buffers with varying ionization enthalpies,<sup>1</sup> and extrapolating the value to zero  $\Delta_{\text{buffer-protonation}}H$ . This process simultaneously gives the net protonation effect for all remaining linked reactions. However, a thorough deconvolution of the energetics of the remaining linked reactions remains complex.

Carbonic anhydrase is a clinically relevant and biochemically well characterized protein.<sup>2</sup> It catalyses hydration–dehydration of carbon dioxide to carbonic acid<sup>3,4</sup> and is involved in vital physiological processes such as pH and CO<sub>2</sub> homeostasis, transport of bicarbonate and CO<sub>2</sub>, biosynthetic reactions, bone resorption, calcification, tumorigenicity, and many other physiological or pathological processes.<sup>5</sup> Therefore, the enzyme is an important target for inhibitors with clinical applications:<sup>6</sup> inhibitors are primarily used as antiglaucoma agents but also for the therapy of various pathologies such as epilepsy and Parkinson's disease.<sup>7</sup>

Carbonic anhydrase has a single active site containing a catalytically active zinc coordinated by three histidine residues and a hydroxide ion (or water molecule) in the resting state. Thermodynamics of metal ion binding to apocarbonic anhydrase has been measured.<sup>8–11</sup> The catalytic mechanism of the enzyme and the mechanism of inhibition has been studied extensively.<sup>12–18</sup> Carbonic anhydrase has been used as a model protein to study molten globules and their refolding (19, 20 and references therein). However, there have been few thermodynamic measurements of sulfonamide inhibitor binding to carbonic anhydrases.<sup>21,22</sup>

## 6.2 Identification of protonation reactions occurring upon binding

The secondary structure of human carbonic anhydrase I is shown in Figure 6.1(a). Beta sheets form a core of carbonic anhydrase, and there are several



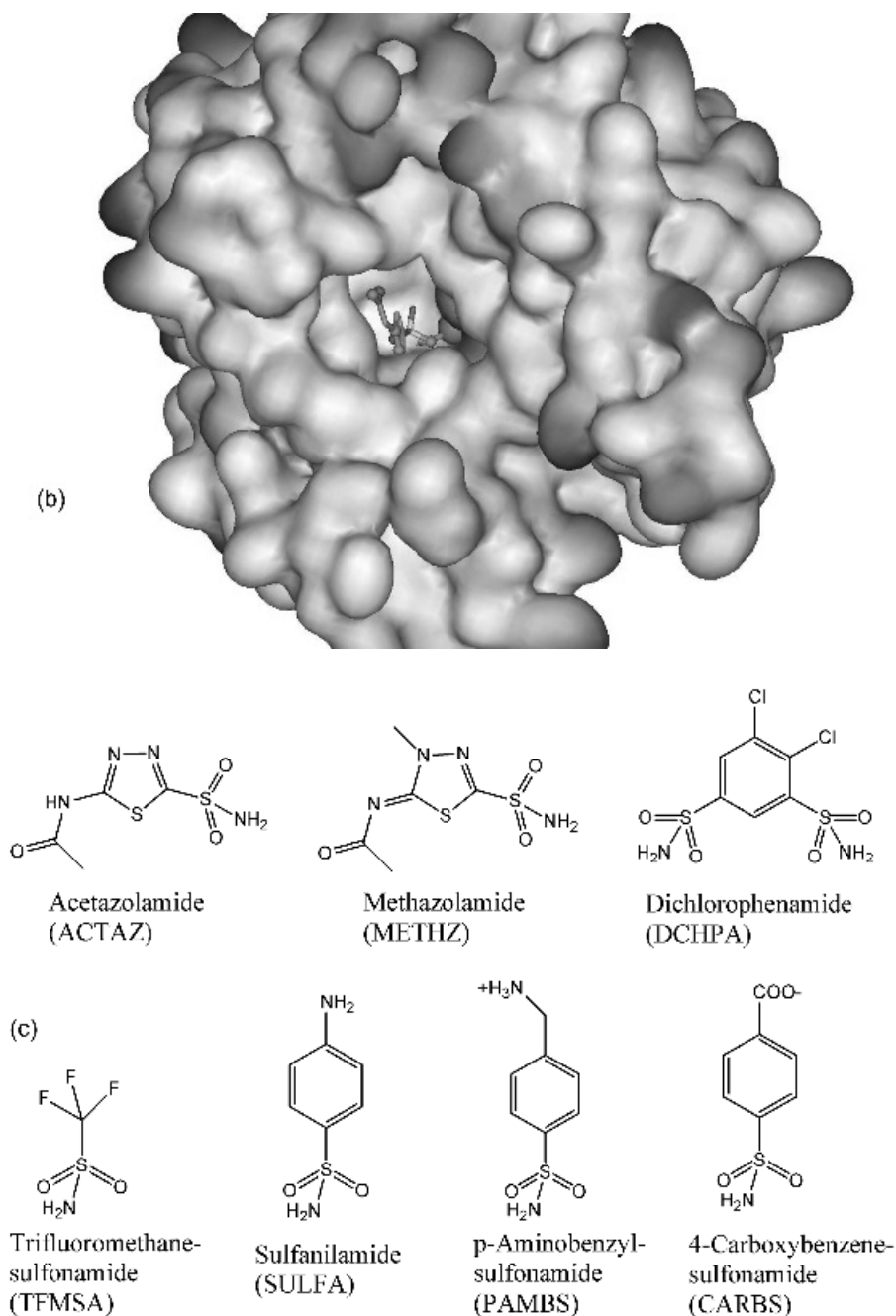
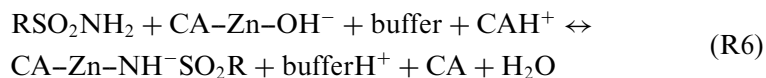
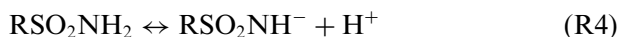
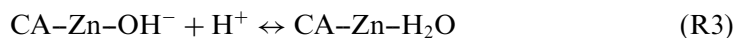


**Figure 6.1** (a) A ribbon view of carbonic anhydrase I showing the secondary structure of the protein with acetazolamide (ball-stick model) bound to the active site zinc atom (large sphere). (b) An electrostatic surface of carbonic anhydrase I drawn using identical orientation and scale as in (a). (c) Chemical structures and abbreviations used in the text of the seven carbonic anhydrase inhibitors reviewed

alpha helices at the edges of the enzyme. Coordinates are from Protein Data Bank 1AZM.pdb. The surface structure is shown in Figure 6.1(b). The large sphere of the zinc atom is positioned deep in the active site cleft. Acetazolamide inhibitor is shown bound in the cleft as a ball–stick model. Crystallographic studies of carbonic anhydrases have recently been reviewed.<sup>23</sup> Chemical structures of the several carbonic anhydrase inhibitors are shown in Figure 1(c). Every inhibitor bears a sulfonamide group, which binds to the zinc atom of the enzyme active site ((a), (b)),<sup>24–26</sup> and the hydrophobic group, which affects the  $pK_a$  of the sulfonamide group and interacts with the hydrophobic pocket of the enzyme. Only the ionized (deprotonated, anionic  $RNH^-$ ) sulfonamide form is thought to bind to the carbonic anhydrase;<sup>22,27</sup> however, most sulfonamide  $pK_a$  values are above seven. Thus, upon binding of most of these inhibitors to carbonic anhydrase, a pH-dependent deprotonation reaction must occur. Likewise, the active site Zn-coordinated hydroxide must protonate prior to being replaced by the amino group of the sulfonamide. Other linked protonation–deprotonation reactions associated with protein side-chains may also occur upon inhibitor binding.<sup>22,27</sup> Such reactions may be summarized as follows (R – inhibitor chemical groups other than sulfonamide, CA – carbonic anhydrase enzyme):



(R1) is a binding reaction, free of protonation–deprotonation contributions (a displacement of water molecule by a deprotonated inhibitor molecule), (R2) is a linked deprotonation or protonation of any ionizable group of the enzyme, (R3) is the protonation of the hydroxide ion coordinated to the active site zinc atom, (R4) is the inhibitor deprotonation, (R5) is buffer protonation, and (R6) is the sum of all the above events. Observed thermodynamic parameters that are measured by an isothermal titration calorimetry (ITC) experiment represent the sum of the linked events (R6). This review describes experiments designed to dissect individual reactions' contributions to the thermodynamic parameters of binding and to correlate them with the structural features of protein–ligand interaction surface.

### 6.3 Observed thermodynamics of inhibitor binding to CA

Figure 6.2 shows typical raw and integrated ITC data for inhibitor binding to carbonic anhydrase. Integrated ITC curves of five inhibitors binding to carbonic anhydrase isozyme II from bovine erythrocytes (b-CAII) are shown in Figure 6.3. Both the cell and the syringe contained 25 mM phosphate buffer, pH 7.0, 50 mM NaCl, and 2 per cent DMSO. Datapoints are experimental ITC data and lines are fitted curves. Inhibitors were ■ – ACTAZ, ◆ – METHZ, ● – TFMSA, ✕ – DCHPA, and ▲ – SULFA. Both the observed

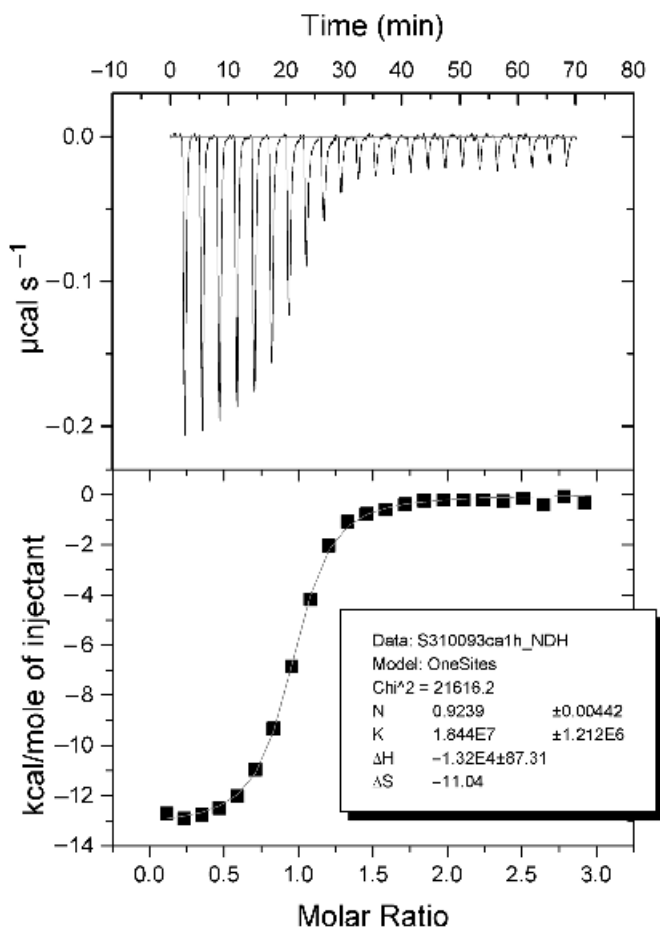


**Figure 6.2** ITC curve (raw data, upper panel) of carbonic anhydrase I (h-CAI) (initial concentration in the cell 3.0 μM) titrated with TFMSA (concentration in the syringe 40 μM, injection size 12.5 μl, injected at 3 minute intervals) at 25°C, where both the cell and syringe contained 20 mM Na phosphate buffer of pH 7.5, 100 mM NaCl, and 0.4 per cent dimethylsulfoxide (DMSO). The lower panel shows the integrated ITC curve of the same data obtained after adding 1.2 kcal mol<sup>-1</sup> for the heat of dilution

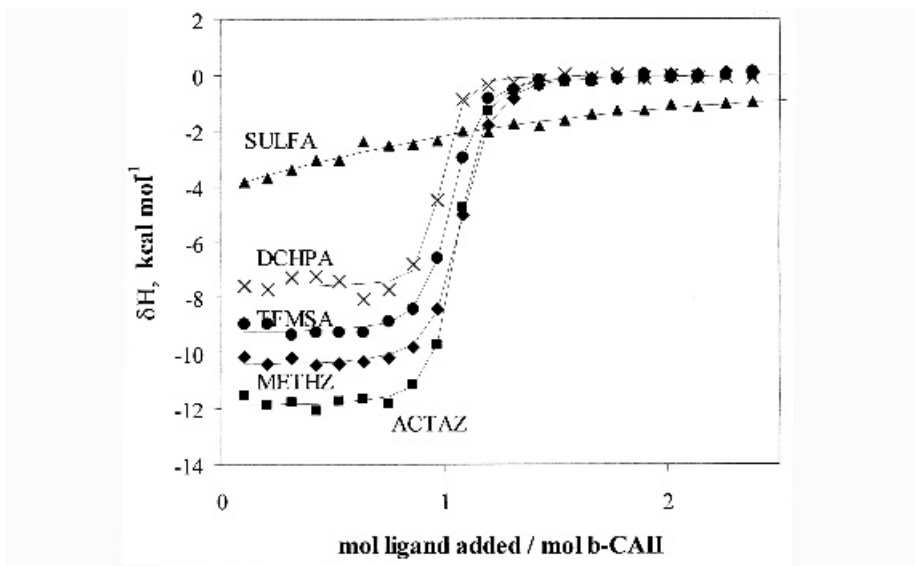


**Figure 6.3** Integrated ITC curves of five inhibitors binding to bovine carbonic anhydrase II at 25°C

enthalpies (initial plateaus of the curves) and the observed binding constants varied significantly depending on the inhibitor. The observed binding constants of the seven inhibitors span a large range, from  $10^3$  to  $10^8 \text{ M}^{-1}$  (Table 6.1) and are specific for each isozyme. Figure 6.4 shows integrated ITC curves of acetazolamide binding to three carbonic anhydrase isozymes. Both the cell and the syringe contained 20 mM phosphate buffer, pH 7.0, 100 mM NaCl, and 1 per cent DMSO. Datapoints are experimental ITC data and lines are curves regressed against the data. Proteins were  $\blacksquare$  – h-CAI,  $\bullet$  – b-CAII, and  $\blacktriangle$  – h-CAII. The observed binding constants varied significantly depending on the protein – h-CAI bound ACTAZ significantly weaker than any CAII, but the observed enthalpies (plateaus of the curves) were quite similar, with less than  $1 \text{ kcal mol}^{-1}$  difference for all three proteins.

Because there is a limit of binding constants that can be determined by ITC (about  $10^8$ – $10^9 \text{ m}^{-1}$  depending on protein concentration), the binding constants of six inhibitors were also measured by a high-throughput thermal shift assay (ThermoFluor<sup>®</sup>) that measures the increase in protein melting temperature in the presence of the inhibitor and has no upper limit to measured affinity.<sup>28–30</sup> A good agreement between the ITC and ThermoFluor<sup>®</sup> data confirmed the accuracy of binding constant determination by ITC, as shown in Figure 6.5. A solid line shows the trend of exact match between the two methods. Open small symbols show binding constants for h-CAI, closed symbols b-CAII, and open large symbols h-CAII. Phosphate buffer of pH 7.0

**Table 6.1** Observed thermodynamic parameters of inhibitor binding to carbonic anhydrases h-CAI, b-CAII, and h-CAII at 37°C representing reactions (R1)–(R4). The enthalpies are extrapolated to zero buffer protonation enthalpy; binding constants were independent of buffer within the error of the experiment

Inhibitor	$K_{\text{b-obs},T_0}$ , <sup>a</sup> M <sup>-1</sup>	$\Delta_{\text{b}}G_{\text{obs},T_0}$ , <sup>b</sup> kcal mol <sup>-1</sup>	$\Delta_{\text{b}}H_{\text{obs},T_0}$ , <sup>c</sup> kcal mol <sup>-1</sup>	$T_0\Delta_{\text{b}}S_{\text{obs},T_0}$ , <sup>d</sup> kcal mol <sup>-1</sup>	$\Delta_{\text{b}}C_p^{\text{obs}}$ , <sup>e</sup> cal mol <sup>-1</sup> K <sup>-1</sup>	$n_{\text{R1-R4}}$ , <sup>f</sup> mol mol <sup>-1</sup>
<i>Carbonic anhydrase I (humans, h-CAI)</i>						
ACTAZ	$8.63 \times 10^5 \pm 1.97 \times 10^5$	$-8.42 \pm 0.13$	$-10.6 \pm 0.3$	$-2.2 \pm 0.3$	$-58 \pm 15$	-0.30
METHZ	$7.61 \times 10^6 \pm 3.13 \times 10^6$	$-9.77 \pm 0.21$	$-9.6 \pm 1.8$	$0.2 \pm 1.8$	$-65 \pm 20$	-0.61
TFMSA	$2.40 \times 10^7 \pm 4.27 \times 10^6$	$-10.47 \pm 0.10$	$-12.6 \pm 0.6$	$-2.0 \pm 0.6$	$-72 \pm 30$	0.29
DCHPA	$8.07 \times 10^5 \pm 4.06 \times 10^5$	$-8.38 \pm 0.25$	$-8.3 \pm 1.6$	$0.1 \pm 1.6$	$-130 \pm 30$	-0.29
SULFA	$6.61 \times 10^3 \pm 6.43 \times 10^3$	$-5.42 \pm 0.42$	$-3.0 \pm 4.0$	$2.4 \pm 4.0$	$-50 \pm 35$	NA
PAMBS	$1.00 \times 10^3 \pm 9.70 \times 10^2$	$-4.26 \pm 0.42$	$-1.0 \pm 5.0$	$3.3 \pm 5.0$	$-50 \pm 0$	NA
<i>Carbonic anhydrase II (bovine, b-CAII)</i>						
ACTAZ	$2.23 \times 10^7 \pm 2.63 \times 10^6$	$-10.43 \pm 0.07$	$-11.5 \pm 1.2$	$-1.0 \pm 1.2$	$-107 \pm 10$	-0.29
METHZ	$1.37 \times 10^7 \pm 1.53 \times 10^6$	$-10.13 \pm 0.07$	$-10.0 \pm 1.6$	$0.1 \pm 1.6$	$-79 \pm 20$	-0.30
TFMSA	$4.10 \times 10^7 \pm 1.41 \times 10^6$	$-10.80 \pm 0.02$	$-9.3 \pm 1.0$	$1.5 \pm 1.0$	$-35 \pm 10$	0.17
DCHPA	$9.83 \times 10^7 \pm 4.55 \times 10^7$	$-11.34 \pm 0.23$	$-7.1 \pm 1.1$	$4.2 \pm 1.1$	$-155 \pm 20$	-0.58
SULFA	$8.90 \times 10^4 \pm 2.97 \times 10^4$	$-7.02 \pm 0.18$	$-5.0 \pm 3.0$	$2.0 \pm 3.0$	$-52 \pm 20$	NA
PAMBS	$2.40 \times 10^4 \pm 8.49 \times 10^3$	$-6.22 \pm 0.19$	$-3.0 \pm 2.8$	$3.2 \pm 2.8$	$-50 \pm 40$	NA
CARBS <sup>g</sup>	$1.06 \times 10^6 \pm 2.4 \times 10^5$	$-8.22 \pm 0.13$	$-10.8 \pm 1.5$	$-2.6 \pm 1.3$	NA	NA
<i>Carbonic anhydrase II (human, h-CAII)</i>						
ACTAZ	$8.23 \times 10^7$	-11.23	-12.5	-1.3	-64	-0.23
METHZ	$2.33 \times 10^7$	-10.45	-11.3	-0.9	-73	-0.22
TFMSA	$4.81 \times 10^7$	-10.90	-12.6	-1.7	-48	0.23
DCHPA	$4.81 \times 10^7$	-10.90	-8.0	2.9	-148	-0.40

<sup>a</sup>Protein-sulfonamide observed binding constant at  $T_0 = 37^\circ\text{C}$ , obtained from ITC experiments. <sup>b</sup>Observed Gibbs free energy of protein-inhibitor binding at  $T_0 = 37^\circ\text{C}$ ,  $\Delta_{\text{b}}G_{\text{obs},T_0} = -RT \ln(K_{\text{b-obs}})$ . <sup>c</sup>Observed enthalpy of protein-inhibitor binding at  $T_0 = 37^\circ\text{C}$ , obtained from ITC experiments and extrapolated to zero enthalpy of buffer ionization. <sup>d</sup>Observed entropy of protein-inhibitor binding at  $T_0 = 37^\circ\text{C}$  ( $T_0\Delta_{\text{b}}S_{\text{obs},T_0} = \Delta_{\text{b}}H_{\text{obs},T_0} - \Delta_{\text{b}}G_{\text{obs},T_0}$ ). <sup>e</sup>Observed heat capacity of protein-inhibitor binding, assumed to be constant in the temperature range of 10–50°C, equal to the slope of the observed enthalpy dependence on temperature. <sup>f</sup>Slopes of the observed enthalpy dependences on the enthalpy of buffer protonation, equal to the net number of linked protonation events. <sup>g</sup>Values for CARBS binding to b-CAII (25°C, phosphate buffer of pH 7.0) were taken from the study by M. Doyle to determine the repeatability of ITC measurements.

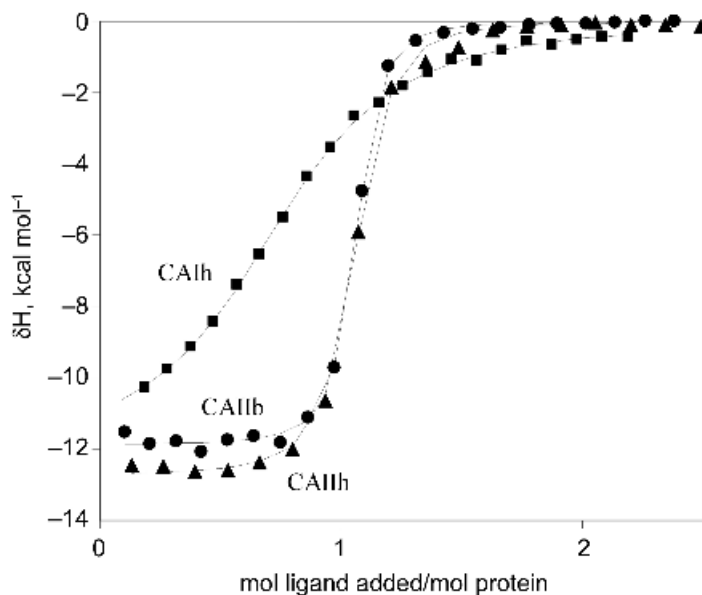


**Figure 6.4** Integrated ITC curves of acetazolamide binding to three carbonic anhydrase isozymes at 25°C

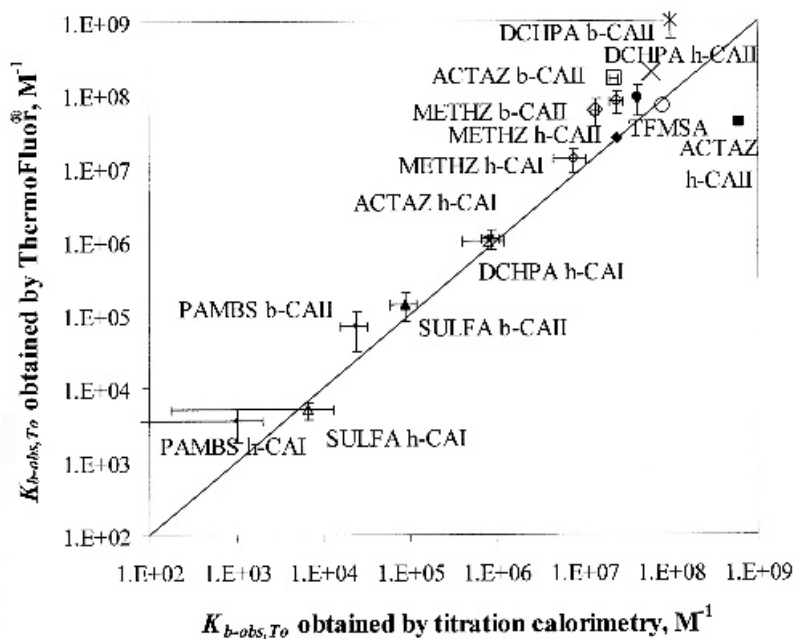


**Figure 6.5** Correlation of the binding constants obtained by ITC and ThermoFluor®

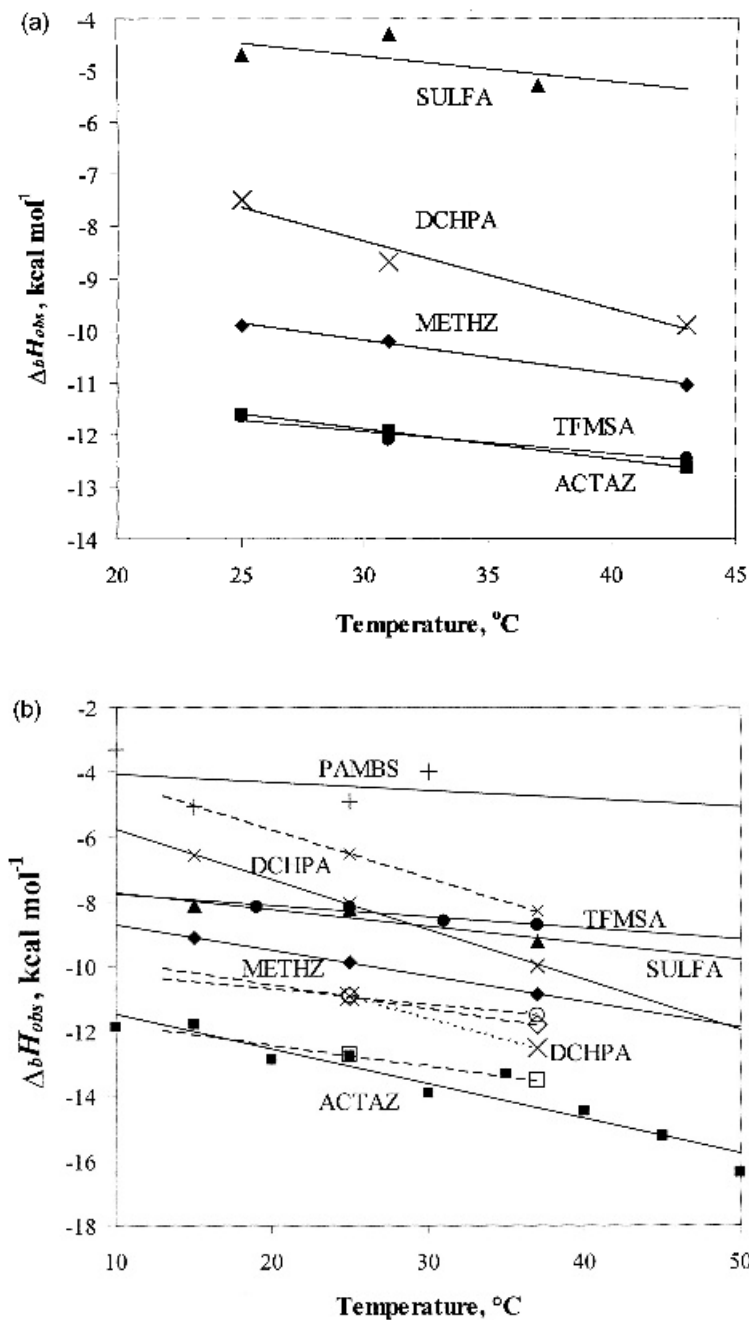


**Figure 6.6** (a) Dependence of observed molar enthalpies of inhibitor binding to h-CAI on temperature (in phosphate buffer, pH 7.0). (b) Temperature dependence of the molar enthalpy of inhibitor binding to CAII (bovine – solid lines, human – dashed lines) as determined by ITC

was used in all cases. Approximate values for ligand binding enthalpy and heat capacity ( $\Delta_b H_{T_0=37^\circ\text{C}} = -5.0 \text{ kcal mol}^{-1}$ ,  $\Delta_b C_p = -300 \text{ cal mol}^{-1} \text{ K}^{-1}$ ) were used to extrapolate estimated  $K_b$  values by ThermoFluor® (accurate at protein melting temperature) to  $37^\circ\text{C}$ . Data for h-CAII are from single determinations and have no error bars.

When an ITC experiment is carried out at several temperatures the heat capacity of the reaction can be obtained from the enthalpy dependence on temperature. Figure 6.6(a) shows the dependence of the observed  $\Delta_{b\text{-obs}}H$  on temperature for isozyme I (Table 6.1). Datapoints are enthalpies of binding as derived from ITC experiments and solid lines are linear fits of the datapoints. Slopes of the linear fits are equal to the observed heat capacity of inhibitor binding to the protein. The heat capacity is assumed to be constant and temperature independent in the range of interest. Inhibitors were: ● – DCHPA, ▲ – METHZ, ■ – ACTAZ, ▲ – SULFA, and ● – TFMSA. Figure 6.6(b) shows the dependence for isozyme II. Datapoints are enthalpies derived from ITC experiment and solid lines are linear fits of the datapoints. Buffers were PIPES for b-CAII buffer (except TFMSA in HEPES), phosphate for h-CAII. For DCHPA, inhibitor data is shown for h-CAII for both phosphate (open diamonds) and Tris (filled diamonds with dotted line). All buffers were of pH 7.0. Inhibitors were ✕ – DCHPA, ◆ – METHZ, ■ – ACTAZ, ▲ – SULFA, ● – TFMSA, and + – PAMBS. This  $\Delta_{b\text{-obs}}C_p$ , however, is also an ‘observed’ value that may be affected by linked protonation events. Thus, attempts to correlate these values to structure and the buried hydrophilic and hydrophobic surface area become dependent on identifying these values.

There are often linked protonation–deprotonation reactions accompanying binding. In order to determine whether such protonation reactions are linked to the binding reaction, the ITC experiment can be carried out in several buffers of different protonation enthalpies. If a net change in protonation occurs, a corresponding change in buffer protonation will add to the observed enthalpy. We have carried out the binding experiments in the following buffers at pH 7.0 (enthalpy of deprotonation at  $37^\circ\text{C}$  is in brackets): phosphate ( $0.70 \text{ kcal mol}^{-1}$ ), PIPES ( $2.79 \text{ kcal mol}^{-1}$ ), MES ( $3.76 \text{ kcal mol}^{-1}$ ), HEPES ( $5.16 \text{ kcal mol}^{-1}$ ), and Tris ( $11.13 \text{ kcal mol}^{-1}$ ). The observed binding constants were found to be buffer independent (within the error of the experiment). However,  $\Delta_{b\text{-obs}}H$  varied greatly depending on the buffer, protein, and the inhibitor. Figure 6.7(a) shows  $\Delta_{b\text{-obs}}H$  for isozyme I as a function of  $\Delta_{\text{buffer-deprotonation}}H$ . Datapoints are experimental ITC data and solid lines are linear fits of the datapoints. Inhibitors were ✕ – DCHPA, ◆ – METHZ, ■ – ACTAZ, and ● – TFMSA. Buffers (25 mM) and the enthalpies of their deprotonation at  $37^\circ\text{C}$  were phosphate  $0.70 \text{ kcal mol}^{-1}$ , PIPES  $2.79 \text{ kcal mol}^{-1}$ , MES  $3.76 \text{ kcal mol}^{-1}$ , HEPES  $5.16 \text{ kcal mol}^{-1}$ , and Tris  $11.13 \text{ kcal mol}^{-1}$ . Figure 6.7(b) shows  $\Delta_{b\text{-obs}}H$  for isozyme II. Datapoints are

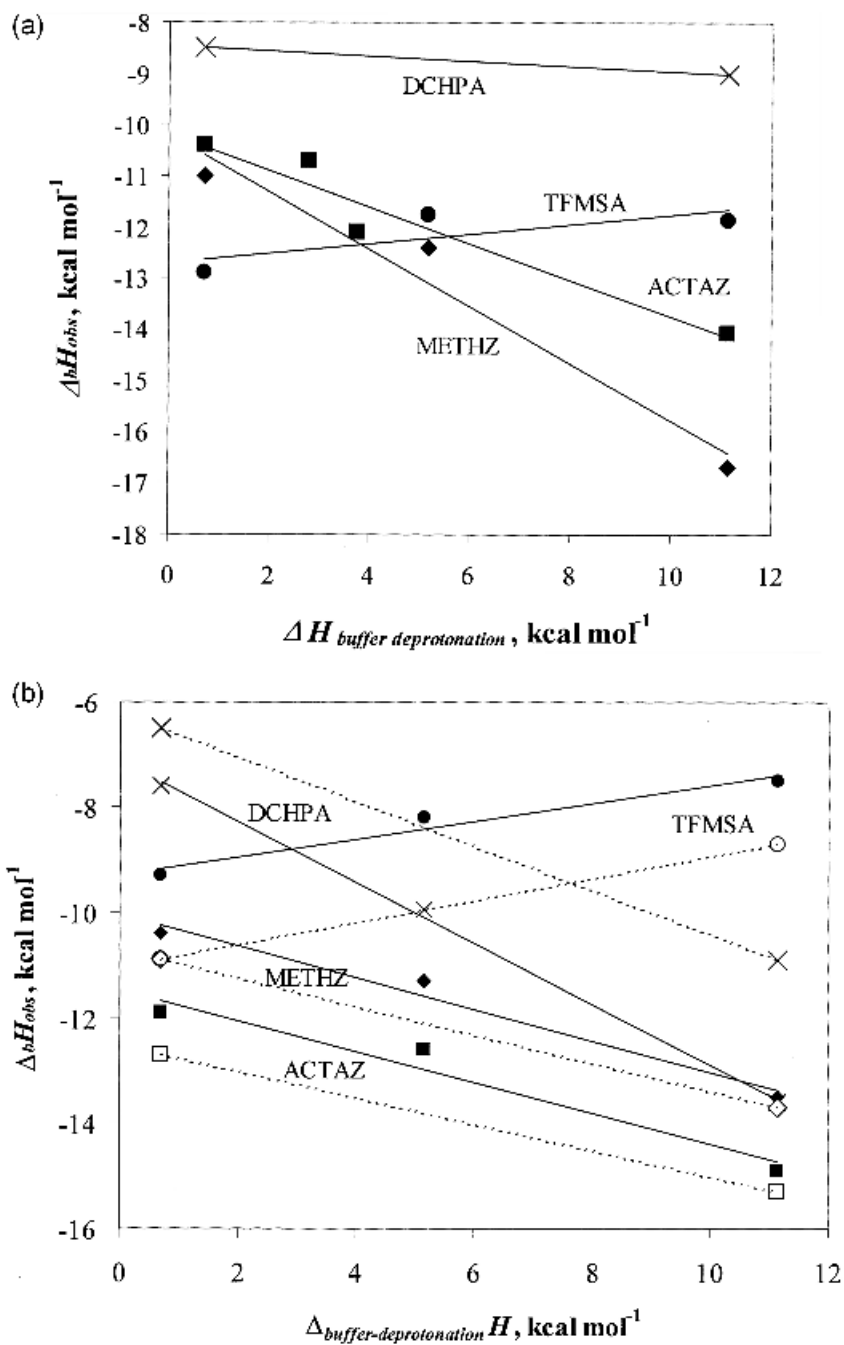


**Figure 6.7** (a) Dependence of molar enthalpies of inhibitor binding to h-CAI on the enthalpy of buffer deprotonation as determined by ITC at 37°C and pH 7.0. (b) Molar enthalpy of inhibitor binding to CAII depends on the enthalpy of buffer deprotonation

enthalpy obtained from ITC experiment and solid lines are linear fits. Solid lines with filled symbols are for b-CAII at 25°C; dashed lines with unfilled symbols are for h-CAII at 25°C. Inhibitors were **X** – DCHPA, **◆** – METHZ, **■** – ACTAZ, and **●** – TFMSA. Only TFMSA binding was coupled with the proton binding; others were linked to proton release. Buffers (25 mM) and the enthalpies of their deprotonation at 25°C were phosphate 1.22 kcal mol<sup>-1</sup>, PIPES 2.74 kcal mol<sup>-1</sup>, MES 3.71 kcal mol<sup>-1</sup>, HEPES 5.02 kcal mol<sup>-1</sup>, and Tris 11.34 kcal mol<sup>-1</sup>. A zero slope in Figure 6.7 indicates no *net* protonation change on binding, while a non-zero slope indicates a linked protonation reaction. A negative slope indicates a *net release* of protons upon ligand binding; a positive slope indicates a *net uptake* of protons.<sup>1</sup> Data in Figure 6.7 gives two important parameters: (1) the slope gives net change in protonation (Table 6.1); (2) the intercept at zero enthalpy of buffer protonation gives buffer-independent binding enthalpies from a collection of  $\Delta_{b-obs}H$  values. Thus, if  $\Delta_{b-obs}H$  represents the sum of (R1)–(R5), (R6), then the intercept gives  $\Delta_bH$  for the sum of (R1)–(R4).

Table 6.1 summarizes observed buffer-independent thermodynamic parameters of seven inhibitors binding to three CA isozymes. When comparing the inhibitors, the observed binding constants spanned a wide range of strengths. However, the underlying mechanism of the large differences between inhibitors is not immediately clear without detailed analysis of all underlying reactions.

Carbonic anhydrase I bound sulfonamide inhibitors consistently more weakly than both isozymes of carbonic anhydrase II. Converted to binding Gibbs free energy,  $\Delta_bG$ , inhibitor affinity varied by 5 kcal mol<sup>-1</sup>, whereas  $\Delta_bH$  varied by more than 8 kcal mol<sup>-1</sup>. When similar experiments were performed with other isozymes (Figure 6.4), an equally large difference in  $\Delta_bG$  and  $\Delta_bH$  was observed (Table 6.1) for a given protein.

The buffer-independent binding enthalpies ((R1)–(R4), Table 6.1) of the seven inhibitors spanned the range from -1 to -12.6 kcal mol<sup>-1</sup>. Typically the carbonic anhydrase, isozyme I, from human erythrocytes (h-CAI)  $\Delta_bG$  was 1–3 kcal mol<sup>-1</sup> less favourable than for the other enzymes. The only deviation from this ranking is trifluoromethanesulfonamide (TFMSA), which bound equally tightly, but with more favourable enthalpy, to h-CAI. Differences between the three proteins were small with the largest difference being for TFMSA: -12.6 kcal mol<sup>-1</sup> for carbonic anhydrase isozyme II from human erythrocytes (h-CAII) and -9.3 kcal mol<sup>-1</sup> for b-CAII. The entropy contributions were smaller than the enthalpies. Entropies of most inhibitors binding were usually positive, especially for b-CAII.

All inhibitors bound with a negative change in heat capacity. The values spanned the range of  $-70 \pm 35$  cal (mol K)<sup>-1</sup> with the exception of DCHPA binding, which gave an approximately double value. DCHPA is the only ligand with two sulfonamide groups and two chlorine atoms. Since  $\Delta_bC_p$

scales with buried hydrophobic surface areas, the greater value possibly arises from the bulkiness of the inhibitor.

The numbers of linked protonation–deprotonation events obtained from the slopes in Figure 6.7 varied from  $-0.61$  to  $+0.29$ . DCHPA, ACTAZ, and METHZ binding was linked to a net release of protons, while the binding of TFMSA was linked to a net uptake of protons. Linked protonation numbers were nearly identical for the two isozymes of CAII.

## 6.4 Energetics of inhibitor protonation

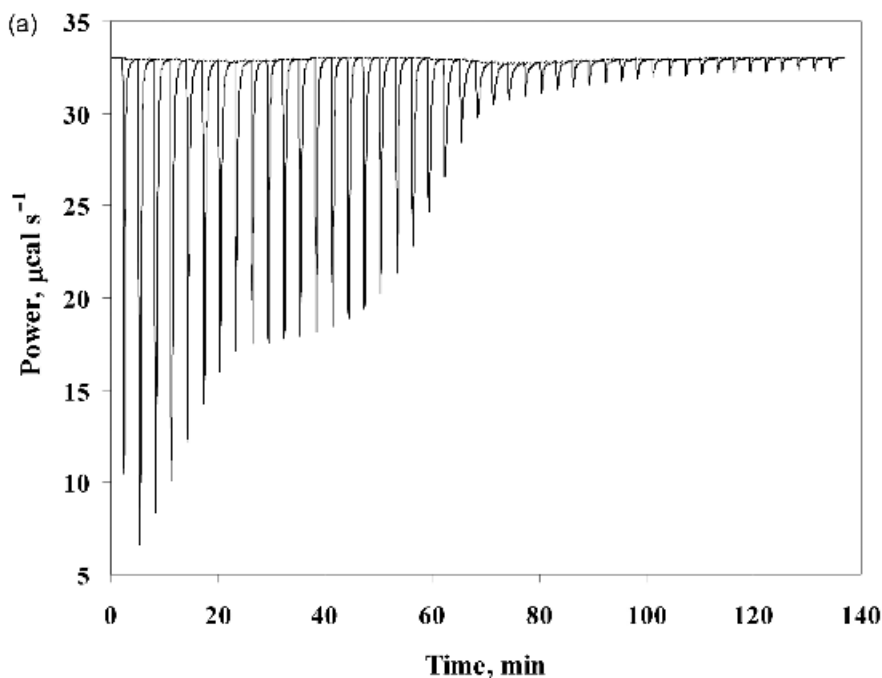
The sulfonamide group of all studied inhibitors may be electrically neutral (protonated  $\text{RNH}_2$ ) or negatively charged (deprotonated  $\text{RNH}^-$ ) as represented in (R4) above. The predominant ionization form of the inhibitor depends on the pH of solution and its  $\text{p}K_a$ . Most sulfonamide inhibitors that do not have strong electron withdrawing groups have  $\text{p}K_a$  values above 7 and thus are usually protonated at physiological pH, thus binding affinity and enthalpy will be pH dependent.

However, only the negatively charged (deprotonated) sulfonamide group is thought to bind to the zinc atom in the active site of carbonic anhydrase.<sup>22</sup> Therefore, inhibitors that exist in a protonated form at pH 7 must undergo a linked deprotonation reaction upon binding to the protein.

In order to understand the effects of inhibitor deprotonation on binding, the energetics of inhibitor protonation were evaluated independently. All seven inhibitors were titrated calorimetrically and potentiometrically with NaOH and HCl to determine the thermodynamics of protonation. Enthalpies and heat capacities were determined by titrating the deprotonated (alkaline) sulfonamides with HCl in the calorimeter, and the Gibbs free energies ( $\text{p}K_a$  values) were determined by potentiometric titration with the pH-meter. The  $\text{p}K_a$  values could not be determined by ITC because the binding constants are out of the range where ITC experiments can determine them accurately.

It was chosen to titrate deprotonated (alkaline) inhibitors with HCl because the reaction of protonation is exothermic and could be determined with greater precision than the reaction of deprotonation with NaOH. Calorimetric titration with NaOH is complicated by a non-trivial behaviour of NaOH dilution. To obtain negatively charged inhibitors, 1.5 molar equivalents of NaOH were added.

Titration curves of inhibitors with HCl exhibit two transitions: (1) an event with stoichiometry 0.5 and  $\Delta_{\text{obs}}H \sim -13 \text{ kcal mol}^{-1}$ , occurring due to neutralization of excess NaOH; (2) an event with stoichiometry 1.0 and inhibitor-dependent enthalpy, occurring due to protonation of the inhibitor sulfonamide group. Figure 6.8(a) shows a titration curve of METHZ with HCl. Concentrations and volumes were identical to pH titration experiments



shown in (c). The first portion of the titration curve represents the reaction between  $\text{H}^+$  and excess  $\text{OH}^-$ . The second portion of the titration curve with the stoichiometry of 1.0 represents inhibitor protonation. Figure 6.8(b) shows titration curves of TFMSA and METHZ with HCl. The enthalpy of the first portion of the titration (stoichiometry  $\sim 0.5$ ,  $\Delta H \sim -13 \text{ kcal mol}^{-1}$ ) is a value close to that expected for the reaction of  $\text{H}^+ + \text{OH}^- \rightarrow \text{H}_2\text{O}$ . The enthalpy of the second portion of the titration curve (stoichiometry  $\sim 1.0$ ) represents the enthalpy of sulfonamide protonation. Heat capacities of sulfonamide protonation were determined by carrying out the titration at several temperatures. The slope of the enthalpy dependence on temperature is equal to the heat capacity of inhibitor protonation.

The exact same solutions and volumes as in the calorimetric experiments were used for potentiometric titration by using a pH-meter. The injection syringe of the VP-ITC calorimeter was used to deliver injections of several microlitres. Such methodology gave high precision titration curves using small volumes of solution. The stoichiometry obtained from potentiometric titration curves precisely matched that obtained from the calorimetric curves. A function describing two transitions was derived according to reference 31 and curves were simulated to match the experimental datapoints. Several representative titration curves are shown in Figure 6.8(c). Concentrations and volumes are identical to those in ITC experiments (panels (a) and (b)). Two transitions are seen: 0.5 equivalent of  $\text{H}^+$  reaction with  $\text{OH}^-$ , and one

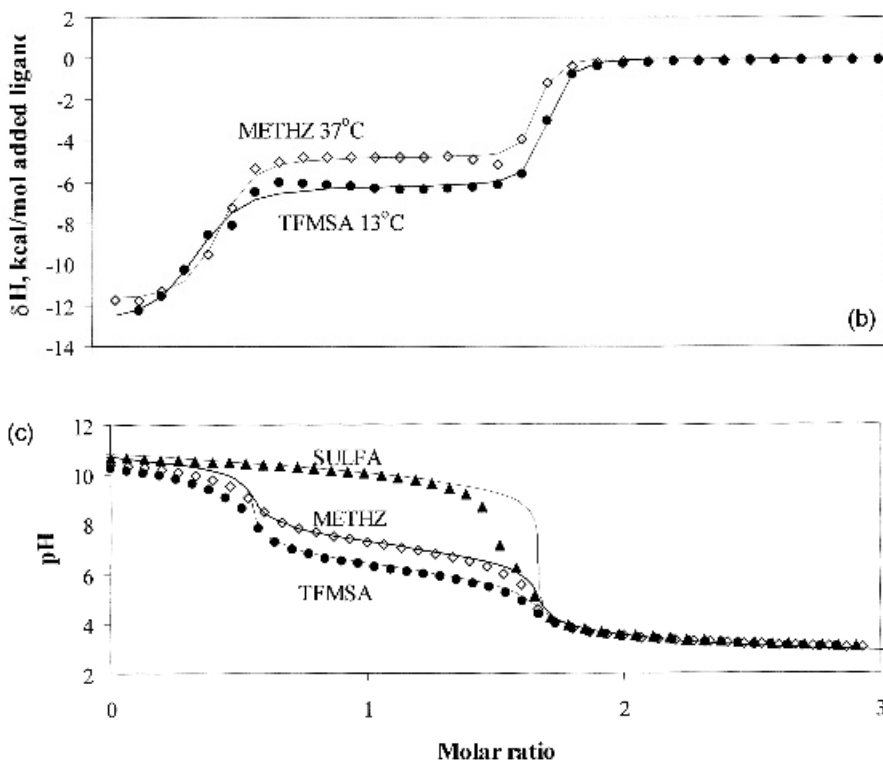


**Figure 6.8** (a) Raw ITC data of METHZ titration with HCl at 25°C is representative of inhibitor protonation enthalpy determinations by ITC, where 1.5 equivalents of NaOH were added to the neutral inhibitor. (b) Examples of integrated ITC curves of TFMSA (●, 13°C) and METHZ (◆, 37°C) titration with HCl. (c) pH titration curves of SULFA (▲), METHZ (◆), and TFMSA (●) at 24°C

equivalent of sulfonamide protonation. The  $pK_a$  is approximately equal to the pH at the midpoint of the second stage of the titration. The midpoint of the second transition closely matches the  $pK_a$  of the inhibitor. A summary of all seven inhibitor protonation energetics is shown in Table 6.2.

Sulfanilamide (SULFA) has the highest  $pK_a$  of all studied inhibitors. Therefore, the fraction of deprotonated sulfonamide at pH 7 is quite small (0.0019) and results in weak affinity (last column in Table 6.2). On the other hand, TFMSA has a  $pK_a$  of 6.02. Therefore, at pH 7 almost all of the inhibitor exists in a negatively charged form (fraction = 0.91). The enthalpies of inhibitor protonation were similar ( $-4.5 \pm 0.5 \text{ kcal mol}^{-1}$ ), except for DCHPA, which was  $-6 \text{ kcal mol}^{-1}$ , perhaps because of two chlorine atoms – electron withdrawing groups – on the phenyl ring. Entropies of protonation were positive and equal to  $16 \pm 2 \text{ cal (mol K)}^{-1}$  for ACTAZ, METHZ, TFMSA, and DCHPA. The remaining three inhibitors have even greater positive entropy of

**Table 6.2** Thermodynamic parameters of inhibitor sulfonamide group protonation (reaction (R4))

Inhibitor	$pK_a$ 25°C, <sup>a</sup> ±0.15	$pK_{a,T_0}$ <sup>b</sup>	$\Delta_{\text{prot}}G_{T_0}$ , <sup>c</sup> kcal mol <sup>-1</sup>	$\Delta_{\text{prot}}H_{T_0}$ , <sup>d</sup> kcal mol <sup>-1</sup>	$T_0\Delta_{\text{prot}}S_{T_0}$ , <sup>e</sup> kcal mol <sup>-1</sup>	$\Delta_{\text{prot}}C_p$ , <sup>f</sup> cal mol <sup>-1</sup> K <sup>-1</sup>	$f_{\text{deprot},T_0}$ at pH 7.0 <sup>g</sup>
ACTAZ	7.30	7.03	-9.98 ± 0.2	-4.5 ± 0.3	5.4 ± 0.5	75 ± 15	0.48
METHZ	7.12	6.86	-9.73 ± 0.2	-4.9 ± 0.2	4.8 ± 0.5	70 ± 20	0.58
TFMSA	6.25	6.02	-8.55 ± 0.2	-4.0 ± 0.3	4.5 ± 0.5	86 ± 10	0.91
DCHPA	8.20	7.89	-11.2 ± 0.2	-6.2 ± 0.4	5.0 ± 0.5	58 ± 30	0.11
SULFA	10.10	9.72	-13.8 ± 0.5	-4.7 ± 2 <sup>h</sup>	9.1 ± 2.5	70 ± 50 <sup>h</sup>	0.084
PAMBS	8.35	8.04	-11.4 ± 0.5	-4.7 ± 2 <sup>h</sup>	6.7 ± 2.5	70 ± 50 <sup>h</sup>	0.084
CARBS	9.60	9.24	-13.1 ± 0.2	-4.1 ± 0.7	9.0 ± 0.5	58 ± 20	0.0057

<sup>a</sup> $pK_a$  measured experimentally by pH titration of the inhibitor as described in the 'Methods' section.<sup>b</sup> $pK_a$  of protonation at 37°C calculated from  $pK_a$  at 25°C, enthalpy, and heat capacity.<sup>c</sup>Gibbs free energy of protonation at 37°C calculated from  $pK_a$  at 37°C.<sup>d</sup>The enthalpy of protonation at 37°C determined by ITC as described in the 'Methods' section.<sup>e</sup> $T_0\Delta_{\text{prot}}S_{T_0}$  at 37°C calculated by subtracting Gibbs free energy from enthalpy.<sup>f</sup>Heat capacity of protonation, obtained from the slope of linear regression of ITC enthalpy dependence on temperature obtained at 13, 25, and 37°C.<sup>g</sup>Fraction of deprotonated sulfonamide at 37°C and at pH 7.0 calculated by Henderson-Hasselbach equation.<sup>h</sup>These values were not determined; they were assumed to be an average of other studied inhibitors, with large uncertainty.

protonation. However, the enthalpies for *p*-aminomethylbenzenesulfonamide (PAMBS) and SULFA were not determined.

Enthalpies of methazolamide protonation have also been determined by measuring the temperature dependence of the  $pK_a$ . The  $pK_a$  of methazolamide protonation was earlier determined to be 7.26,<sup>22</sup> close to our determined value of 7.12 at 25°C. Our measured enthalpy of methazolamide protonation of  $-5.8 \text{ kcal mol}^{-1}$  was close to the value of  $-7.0 \text{ kcal mol}^{-1}$  at 25°C.<sup>22</sup> The  $pK_a$  of acetazolamide has been previously determined to be 7.2,<sup>12</sup> and we obtained a value of 7.30.

## 6.5 Sulfonamide ‘anion’ binding thermodynamics

The process of inhibitor protonation (R4) can now be subtracted from the buffer-independent values ((R1)–(R4), Table 6.1), giving the thermodynamic parameters for reactions (R1)–(R3).

To obtain the binding constant independent of inhibitor protonation ( $K_{b,T_0}$ ), the observed binding constant ( $K_{b\text{-obs},T_0}$ ) was divided by the fraction of deprotonated sulfonamide ( $f_{\text{deprot}}$ , Table 6.2), present at pH 7.0:

$$K_{b,T_0} = \frac{K_{b\text{-obs},T_0}}{f_{\text{deprot}}} \quad (1)$$

The enthalpies of deprotonated sulfonamide binding to carbonic anhydrases were calculated from:

$$\Delta_b H_{T_0} = \Delta_{b\text{-obs}} H_{T_0} + \Delta_{\text{prot}} H_{T_0} (1 - f_{\text{deprot}}) \quad (2)$$

where  $\Delta_{\text{prot}} H_{T_0}$  is the enthalpy of sulfonamide protonation. The observed enthalpies of ligand binding ( $\Delta_{b\text{-obs}} H_{T_0}$ ) are the ones obtained after extrapolating to zero buffer protonation enthalpy. Similarly, the ligand protonation-independent heat capacity of binding was estimated from:

$$\Delta_b C_{p,T_0} = \Delta_{b\text{-obs}} C_{p,T_0} + \Delta_{\text{prot}} C_{p,T_0} (1 - f_{\text{deprot}}) \quad (3)$$

A summary of the inhibitor binding data after accounting for inhibitor deprotonation (R1)–(R3) is listed in Table 6.3. The data is most precise for the four strongly binding ligands as seen from the standard deviation and uncertainty of the data.

Unexpected conclusions were drawn from the Table 6.3. After consideration of fractions of deprotonated inhibitor, the inhibitors bound to each carbonic anhydrase with similar affinities, differing by less than one order of magnitude. Such a large reduction in the difference of observed binding constants was unexpected when considering that the observed binding constants varied by four orders of magnitude (from  $7 \times 10^3$  to  $2 \times 10^7$ ) for h-CAI and three orders of magnitude (from  $9 \times 10^4$  to  $1 \times 10^8$ ) for b-CAII

**Table 6.3** Thermodynamic parameters of inhibitor binding to carbonic anhydrases h-CAI, b-CAII, and h-CAII at 37°C calculated from data in Tables 6.1 and 6.2 to represent reactions (R1)–(R3). This data represents the thermodynamic parameters of ‘anionic’ sulfonamide binding

Inhibitor	$K_b, T_0^a, M^{-1}$	$\Delta_b G_{T_0}^b,$ kcal mol <sup>-1</sup>	$\Delta_b H_{T_0}^c,$ kcal mol <sup>-1</sup>	$T_0 \Delta_b S_{T_0}^d,$ kcal mol <sup>-1</sup>	$\Delta_b C_p^e,$ cal mol <sup>-1</sup> K <sup>-1</sup>	$n_{R1-R3}^f,$ mol mol <sup>-1</sup>
<i>Carbonic anhydrase I (humans, h-CAI)</i>						
ACTAZ	$1.79 \times 10^6 \pm 8.37 \times 10^5$	$-8.87 \pm 0.24$	$-12.9 \pm 0.4$	$-4.1 \pm 0.4$	$-97 \pm 21$	0.41
METHZ	$1.31 \times 10^7 \pm 7.91 \times 10^6$	$-10.10 \pm 0.29$	$-11.5 \pm 1.8$	$-1.4 \pm 1.8$	$-94 \pm 28$	1.03
TFMSA	$2.66 \times 10^7 \pm 1.16 \times 10^7$	$-10.54 \pm 0.22$	$-12.9 \pm 0.6$	$-2.4 \pm 0.7$	$-80 \pm 32$	-0.20
DCHPA	$7.11 \times 10^6 \pm 4.86 \times 10^6$	$-9.72 \pm 0.32$	$-12.3 \pm 1.6$	$-2.6 \pm 1.6$	$-181 \pm 42$	1.18
SULFA	$3.48 \times 10^6 \pm 3.39 \times 10^6$	$-9.28 \pm 0.42$	$-7.5 \pm 4.0$	$1.8 \pm 4.1$	$-120 \pm 61$	NA
PAMBS	$1.19 \times 10^4 \pm 1.16 \times 10^4$	$-5.79 \pm 0.42$	$-5.2 \pm 5.0$	$0.6 \pm 5.0$	$-64 \pm 50$	NA
<i>Carbonic anhydrase II (bovine, b-CAII)</i>						
ACTAZ	$4.61 \times 10^7 \pm 1.89 \times 10^7$	$-10.88 \pm 0.21$	$-13.8 \pm 1.2$	$-2.9 \pm 1.2$	$-146 \pm 18$	0.81
METHZ	$2.35 \times 10^7 \pm 9.55 \times 10^6$	$-10.46 \pm 0.21$	$-11.9 \pm 1.6$	$-1.5 \pm 1.6$	$-108 \pm 28$	0.72
TFMSA	$4.53 \times 10^7 \pm 1.75 \times 10^7$	$-10.87 \pm 0.20$	$-9.7 \pm 1.0$	$1.1 \pm 1.0$	$-43 \pm 14$	-0.08
DCHPA	$8.66 \times 10^8 \pm 5.62 \times 10^8$	$-12.68 \pm 0.31$	$-11.1 \pm 1.1$	$1.5 \pm 1.2$	$-206 \pm 36$	1.47
SULFA	$4.69 \times 10^7 \pm 2.55 \times 10^7$	$-10.89 \pm 0.27$	$-9.5 \pm 3.0$	$1.4 \pm 3.1$	$-122 \pm 54$	NA
PAMBS	$2.86 \times 10^5 \pm 1.60 \times 10^5$	$-7.74 \pm 0.27$	$-7.2 \pm 2.8$	$0.6 \pm 2.9$	$-114 \pm 64$	NA
CARBS	$1.69 \times 10^8$	$-11.23$	$-15.6$	$-4.4$	NA	NA
<i>Carbonic anhydrase II (human, h-CAII)</i>						
ACTAZ	$1.71 \times 10^8$	$-11.68$	$-14.9$	$-3.2$	$-114$	0.77
METHZ	$3.99 \times 10^7$	$-10.79$	$-13.4$	$-2.6$	$-113$	0.64
TFMSA	$5.31 \times 10^7$	$-10.96$	$-12.9$	$-2.0$	$-61$	-0.14
DCHPA	$4.23 \times 10^8$	$-12.24$	$-13.5$	$-1.2$	$-203$	1.29

<sup>a</sup>Binding constant obtained by dividing the observed binding constant at  $T_0 = 37^\circ\text{C}$ , from Table 6.1, by the fraction of deprotonated sulfonamide at pH 7.0 (from Table 6.2),  $K_b, T_0 = K_{b-obs, T_0} / f_{deprot}$ . <sup>b</sup>Gibbs free energy of deprotonated inhibitor binding to protein at  $T_0 = 37^\circ\text{C}$ ,  $\Delta_b G_{T_0} = -RT \ln(K_b)$ . <sup>c</sup>Enthalpy of protein-inhibitor binding at  $T_0 = 37^\circ\text{C}$ , obtained from ITC experiments and accounting for the enthalpy of inhibitor deprotonation according to Formula (6.2). <sup>d</sup>Entropy of protein-inhibitor binding at  $T_0 = 37^\circ\text{C}$  ( $T_0 \Delta_b S_{T_0} = \Delta_b H_{T_0} - \Delta_b G_{T_0}$ ). <sup>e</sup>Heat capacity of protein-inhibitor binding, constant in the temperature range of 10–50°C, calculated according to Formula (6.3). <sup>f</sup>Slopes of the observed enthalpy dependences on the enthalpy of buffer protonation equal to the net number of linked protonation events for reactions (R1)–(R3) calculated by subtracting observed  $n$  (Table 6.1) from the fraction of protonated sulfonamide (Table 6.2) lists fractions of deprotonated sulfonamide).

(excluding PAMBS, where binding constants were not sufficiently accurately determined). The largest portion of the observed difference in affinity lies with the difference of sulfonamide protonation thermodynamics and not with the differences of surface interactions between the inhibitors and protein.

For all ligands, the binding remained enthalpy driven after accounting for inhibitor protonation. The entropy contribution was even closer to zero after accounting for inhibitor deprotonation. The heat capacities became significantly more negative than the buffer-independent values in Table 6.1. DCHPA remained an inhibitor with about twice the negative heat capacity of other inhibitors.

## 6.6 Correlations between structures and the thermodynamics of sulfonamide binding to CA

Co-crystal structures of several sulfonamide inhibitors bound to human carbonic anhydrase I and II isozymes have been solved.<sup>23,32,33</sup> Sequence alignments of the amino acid residues participating in the direct contact with the site where sulfonamide inhibitors bind is shown in Table 6.4. The numbering is that of h-CAI. Amino acids were selected if they are located within  $\sim 4.5$  Å of any ligand in the structures shown in Figure 6.9. Sequences are taken from the Swiss-Prot database and reference 2. The first three enzymes are where there are crystal structures and our experimental data are separated from other sequences by a horizontal line. Sequences where no crystal structures are available were aligned through homology. Histidines 94,

**Table 6.4** Amino acid sequence structural alignment of selected carbonic anhydrase enzyme active site region

	91	94	96	119	121	131	143	198	199	200	209
h-CAI	F	H	H	H	A	L	V	L	T	H	W
h-CAII	I	H	H	H	V	F	V	L	T	T	W
b-CAII	V	H	H	H	L	F	V	L	T	T	W
h-CA3	R	H	H	H	V	F	V	F	T	T	W
h-CA4	K	H	H	H	V	V	V	L	T	T	W
h-CA5	K	H	H	H	V	Y	V	L	T	T	W
h-CA6	Q	H	H	H	V	Y	V	L	T	T	W
h-CA7	K	H	H	H	V	F	V	L	T	T	W
h-CA9	L	H	H	H	V	D	L	L	T	T	W
h-CA12	T	H	H	H	V	A	V	L	T	T	W
h-CA13	R	H	H	H	V	F	V	L	T	V	W
h-CA14	A	H	H	H	V	F	V	L	T	V	W

96, and 119 are conserved among all members because they are bound to the catalytic zinc atom. Also conserved are Thr199 and Trp209. Threonine 199 is thought to be crucial for the alignment of bound carbon dioxide, because the mutation of threonine into any amino acid (except serine) diminished catalytic activity by more than two orders of magnitude.<sup>34</sup>

Thermodynamic parameters listed in Table 6.3 represent the sum of reactions (R1), (R2), and (R3). They are not the ‘true’ parameters of reaction (R1). However, reactions (R2) and (R3) cannot be subtracted from (R1) without their independent experimental measurement. It has been hypothesized that the  $pK_a$  of the water molecule bound to zinc–CA is the same as that bound to cobalt–CA, and that the enthalpies of protonation are the same.<sup>22</sup> Here we do not make such assumptions.

Figure 6.9 shows the following structures of the active site region. Portions of protein amino acids directly interacting with the ligand or otherwise important for visualization of the active site are shown in sticks. Atoms that have relatively close distances between the ligand and protein are shown in not-up-to-scale CPK mode. The active site zinc atom is shown in up-to-scale CPK mode. The models are drawn with Web Lab Viewer Lite 4.2 software. Amino acid numbers are the same as in Table 6.4, sequence alignment. (a) shows h-CAI complexed with hydrocarbonate (1HCB). Bicarbonate is bound by two hydrogen bonds to Thr199, similar to how sulfonamides bind. This structure is included to show that the overall positions of all amino acids involved in contacts with ligands are in essentially the same orientation as in structures with bound sulfonamide ligands. (b) shows h-CAI with acetazolamide (1AZM). The relatively bulky ACTAZ ligand is within contact to all amino acid groups shown in ball and stick. Two hydrogen bonds are formed to Thr 199; the rest are essentially hydrophobic van der Waals contacts. (c) shows h-CAI with methazolamide (1BZM). The structure is very similar to the structure of h-CAI with bound ACTAZ ligand. The only significant difference is that His200 is in steric contact with the extra methyl group of the METHZ ligand and, therefore, the His200 side chain is slightly rotated as compared to the ACTAZ structure. (d) shows h-CAI with sulfanilamide (in the presence of mercury, 1CZM). SULFA is a smaller ligand than ACTAZ or METHZ; therefore, it does not make contact with Leu131. The rest of the structure is similar to ACTAZ and METHZ. (e) shows h-CAII complexed with bromide (1RAZ). This structure is included as a reference to the structure of h-CAII with TFMSA. All amino acids are in nearly identical positions as when TFMSA is bound instead of bromide. (f) shows h-CAII with trifluoromethanesulfonamide (1BCD). TFMSA is bound by two hydrogen bonds to Thr 199, and the zinc atom by an ionic bond. TFMSA is a relatively small ligand and it fits into a small space between Leu198 and Trp209, where no other sulfonate ligands of this study could fit. Therefore, TFMSA is in a different orientation than other sulfonamides.

All bound sulfonamide inhibitors form an ionic bond with zinc atom and two hydrogen bonds to threonine 199: between the sulfonamide N and the backbone carbonyl, and between an O and Thr 200 backbone amide. METHZ, ACTAZ, and SULFA are oriented outwards, pointing towards the solvent with their hydrophobic moiety. TFMSA, however, is oriented differently, with fluorine atoms pointing towards the tryptophan 209. Only the relatively small molecule of TFMSA could fit in such an orientation. Therefore, TFMSA, as the smallest inhibitor in this study, is the only one that does not reach Ile91 or Phe91 in any of the isozymes. A co-crystal structure with TFMSA is available only for h-CAII. The exact mode of TFMSA binding to the other two enzymes is assumed to be in the same orientation as with h-CAII.

Trifluoromethane sulfonamide bound with similar binding constants to all three carbonic anhydrases (Table 6.3). However, the enthalpies of binding, which were identical for h-CAI and h-CAII ( $-12.9 \text{ kcal mol}^{-1}$ ), were less favourable for b-CAII ( $-9.7 \text{ kcal mol}^{-1}$ ). This difference may be associated with either His200, which is Thr in b-CAII, amino acid 121 (Ala in h-CAI, Val in b-CAII, and Leu in h-CAII), or some group external to the active site. Most likely, the difference is due to His200, which is in direct contact with TFMSA.

Other studied inhibitors bound significantly more strongly to CAII than to CAI. Active sites of the two carbonic anhydrases are structurally very similar. The following amino acids differ (Table 6.4) among h-CAI, h-CAII, and b-CAII near the active site based on sequence homology:<sup>23</sup> F91(h-CAI)–I91(h-CAII)–V91(b-CAII), A121–V121–L121, L131–F131–F131, H200–T200–T200. These differences may account for the differences in thermodynamics of inhibitor binding.

When comparing ACTAZ with METHZ, which differs by only one methyl group, we see that ACTAZ binds more strongly than METHZ to both CAII, but METHZ binds stronger to CAI than to both CAII. This difference cannot be explained by the difference of the amino acid in position 200. Most likely the difference lies with the amino acids in positions 91, 121, and 131. When comparing the enthalpies of ACTAZ and METHZ binding to the three enzymes, the enthalpy is most negative for h-CAII and least negative for h-CAI. Another difference between ACTAZ and METHZ is in the linked deprotonation reaction of h-CAI. There is no such difference, however, for h-CAII and b-CAII. The first explanation of such a difference is that His200 in h-CAI changes its  $pK_a$  upon METHZ binding, but not on ACTAZ binding. The methyl group present in METHZ is located so close to His200 in h-CAI (Figure 9(c)) that the His side chain is significantly rotated. Experimentally, we observe that h-CAI exhibits such a linked protonation reaction, whereas both h-CAII and b-CAII, which have Thr instead of His, do not exhibit such a linked protonation reaction.

PAMBS is structurally very similar to SULFA. They differ by only one methyl group, which causes the PAMBS amino group to be positively charged

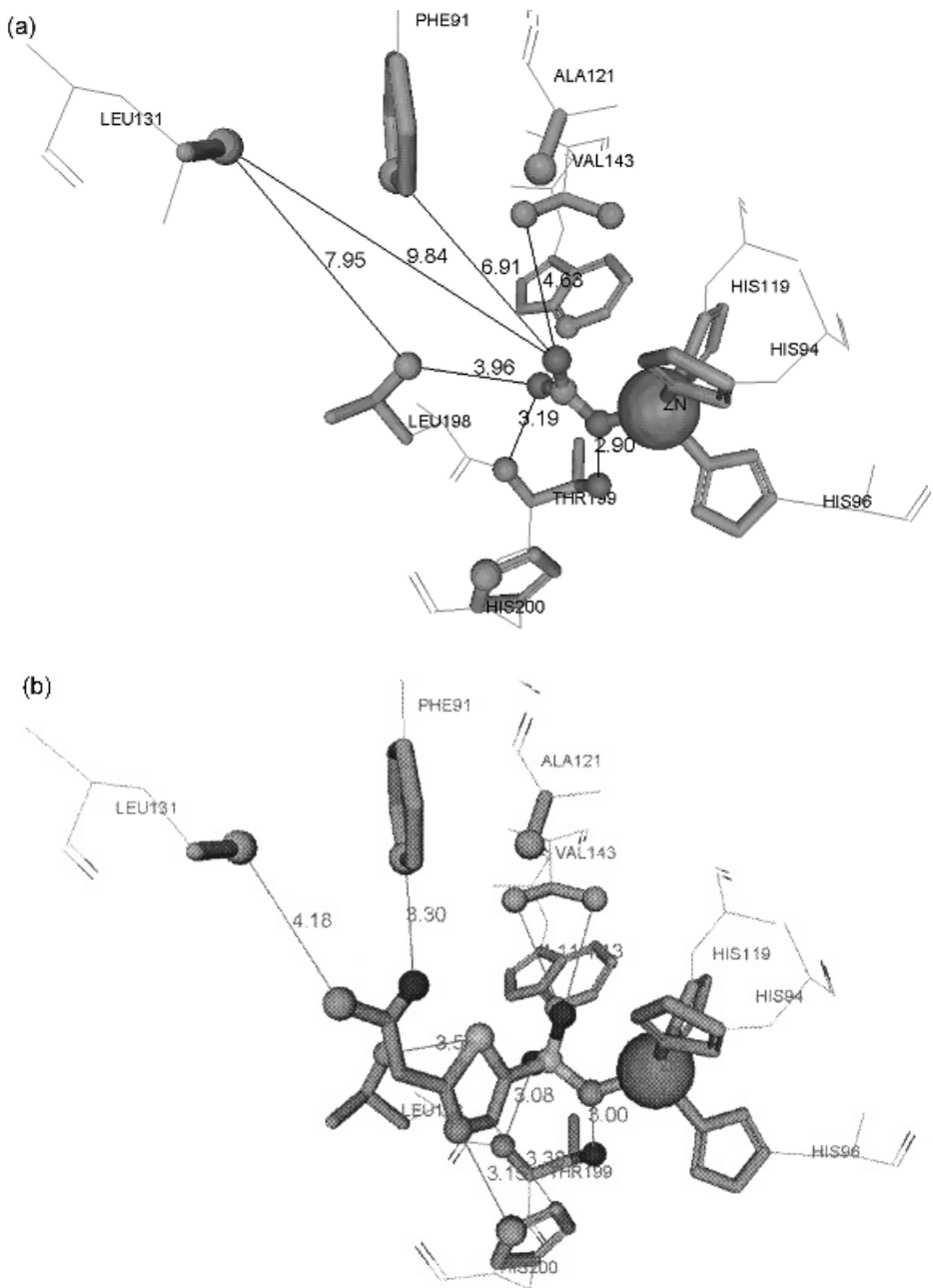


**Figure 6.9** The structures of the active site regions of human carbonic anhydrase I (panels a–d) and II (human, panels e, f) with bound inhibitors. (a) h-CAI with bound bicarbonate (PDB code 1HCB). (b) h-CAI with bound acetazolamide (ACTAZ, 1AZM). (c) h-CAI with bound methazolamide (METHZ, 1BZM). (d) h-CAI with bound sulfanilamide in the presence of Hg (SULFA, 1CZM). (e) h-CAII with bound bromide anion (1RAZ). (f) h-CAII with bound trifluoromethanesulfonamide (TFMSA, 1BCD)

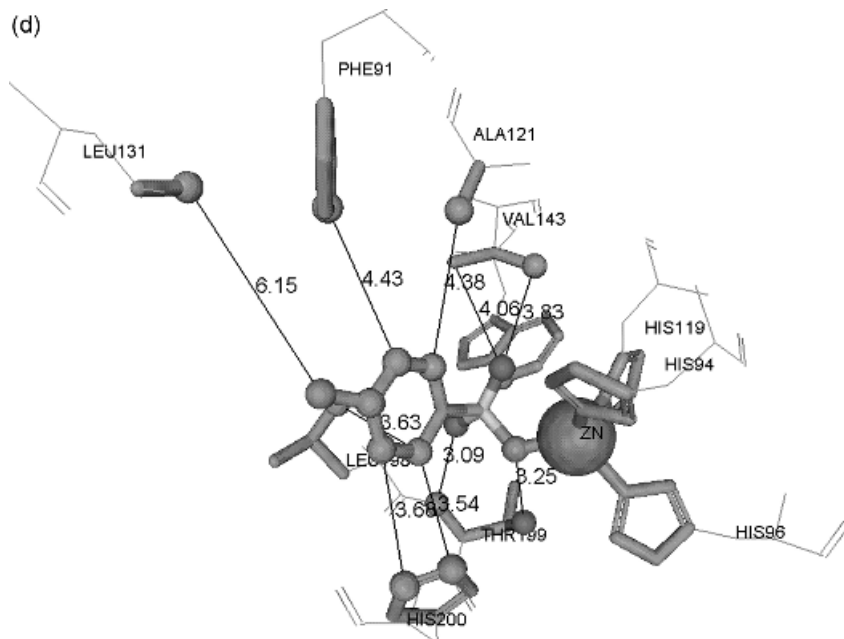
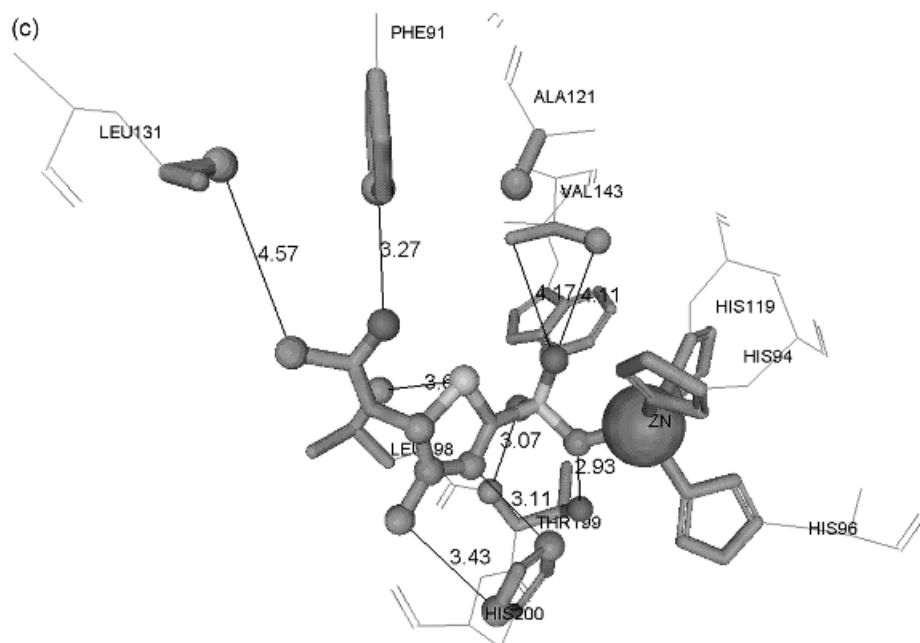


Figure 6.9 (continues)

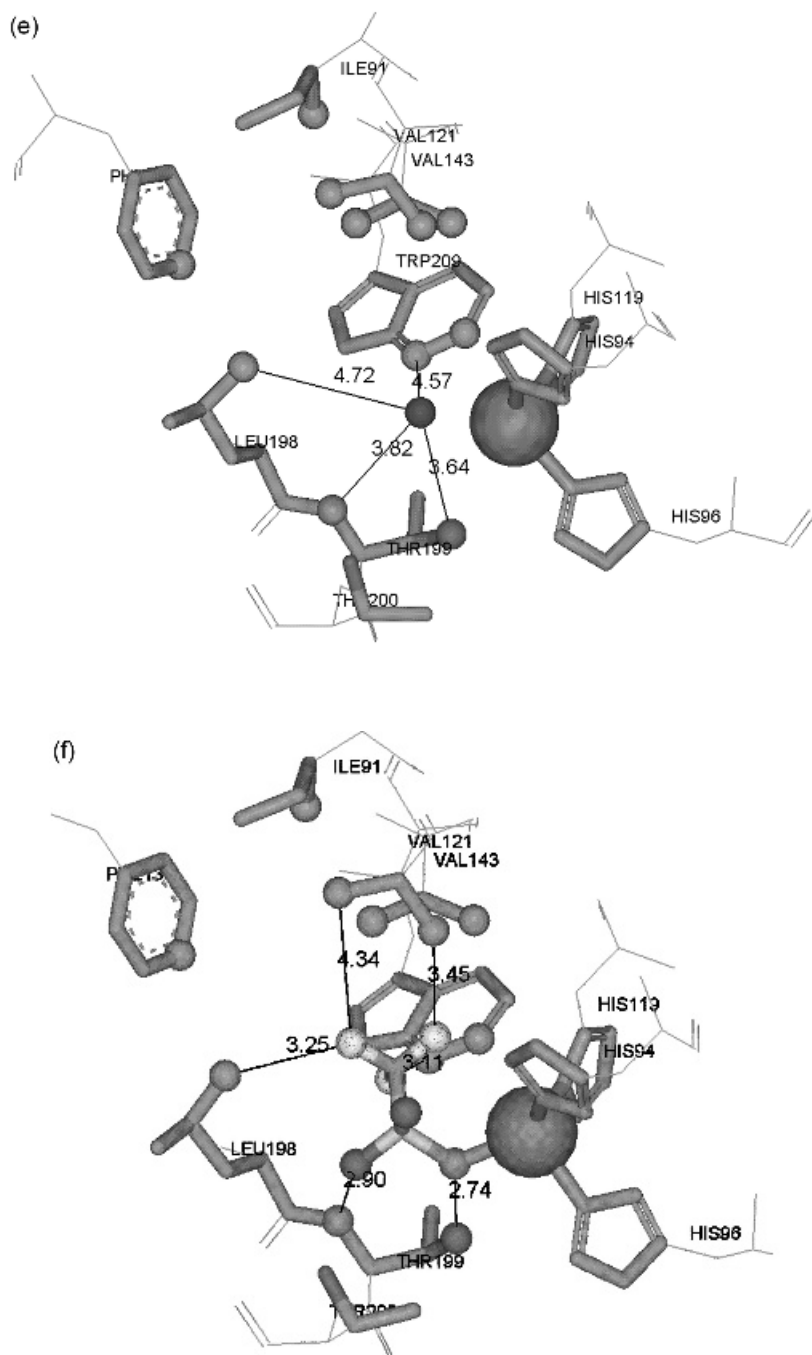


Figure 6.9 (continued)

at pH 7.0. This difference is entirely enthalpic and causes over 100-fold reduction in binding constant from SULFA to PAMBS. The positive charge reduces the sulfonamide  $pK_a$  from 10.10 (SULFA) to 8.35 (PAMBS), making the binding tighter. Therefore, the presence of the positive charge on the amino group of PAMBS reduces the affinity to carbonic anhydrase by about four orders of magnitude.

The binding of 4-carboxybenzene sulfonamide (CARBS) to bovine carbonic anhydrase II has recently been studied by a number of laboratories worldwide with the goal of determining statistical uncertainty of titration calorimetry and other data.<sup>35</sup> At pH 7.0 this inhibitor has additional negative charge on the carboxylic group, making it a significantly stronger binder than the structurally similar SULFA or PAMBS. Interestingly, the enthalpy obtained after accounting for the inhibitor deprotonation is the most negative of all inhibitors in this study, consistent with additional specific interactions.

## 6.7 Conclusions

1. Dissection of all contributing reactions to the observed thermodynamics of inhibitor binding to a protein is necessary in order to correlate the thermodynamic parameters with the structure of the protein–ligand complex.
2. Sulfonamide inhibitors bound more strongly to both CAII than to CAI. An especially large difference of over two orders of magnitude was observed for dichlorophenamide. The smallest difference among the three enzymes was observed for TFMSA and METHZ binding.
3. The major difference in affinities of the inhibitors lies within the differences of sulfonamide group  $pK_a$  values. After accounting for the deprotonation of the ligand, the range of binding constants for the inhibitors was reduced from four to one order of magnitude.
4. For all ligands, the binding was enthalpy driven, especially for the most tightly binding ligands. After accounting for the enthalpic contribution to sulfonamide deprotonation and the sulfonamide  $pK_a$ , the binding enthalpy was much more similar among inhibitors.
5. The change in heat capacity of binding was negative, consistent with the burial of hydrophobic surfaces upon binding. Heat capacity of protonation was positive, thus making the heat capacity of binding even more negative after accounting for inhibitor deprotonation.

## References

1. Baker BM and Murphy KP. (1996) *Biophys. J.* **71**(4): 2049–2055.
2. Sly WS and Hu PY. (1995) *Annu. Rev. Biochem.* **64**: 375–401.
3. Lindskog S. (1997) *Pharmacol. Ther.* **74**: 1–20.
4. Thoms S. (2002) *J. Theor. Biol.* **215**: 399–404.
5. Casini A, Scozzafava A, Mastrolorenzo A and Supuran LT. (2002) *Curr. Cancer Drug Targets* **2**: 55–75.
6. Mattioni BE and Jurs PC. (2002) *J. Chem. Inf. Comput. Sci.* **42**: 94–102.
7. Masereel B, Rolin S, Abbate F, Scozzafava A and Supuran CT. (2002) *J. Med. Chem.* **45**: 312–320.
8. Henkens RW, Watt GD and Sturtevant JM. (1969) *Biochemistry* **8**: 1874–1878.
9. DiTusa CA, Christensen T, McCall KA, Fierke CA and Toone EJ. (2001) *Biochemistry* **40**: 5338–5344.
10. DiTusa CA, McCall KA, Christensen T, Mahapatro M, Fierke CA and Toone EJ. (2001) *Biochemistry* **40**: 5345–5351.
11. Hunt JA, Ahmed M and Fierke CA. (1999) *Biochemistry*, **38**: 9054–9062.
12. Mansoor UF, Zhang XR and Blackburn GM. (2000) *Exs*: 437–459.
13. Nair SK, Krebs JF, Christianson DW and Fierke CA. (1995) *Biochemistry* **34**: 3981–3989.
14. Abbate F, Supuran CT, Scozzafava A, Orioli P, Stubbs MT and Klebe G. (2002) *J. Med. Chem.* **45**: 3583–3587.
15. Baird TT Jr, Waheed A, Okuyama T, Sly WS and Fierke CA. (1997) *Biochemistry* **36**: 2669–2678.
16. Doyon JB, Hansen EA, Kim CY, Chang JS, Christianson DW, Maddar RD, Voet JG, Baird TA Jr, Fierke CA and Jain A. (2000) *Org. Lett.* **2**: 2557–2558.
17. Maddar RD, Kim CY, Chandra PP, Doyon JB, Baird TA Jr, Fierke CA, Christianson DW, Voet JG and Jain A (2002) *J. Org. Chem.* **67**: 582–584.
18. Tripp BC, Smith K and Ferry JG (2001) *J. Biol. Chem.* **276**: 48615–48618.
19. Carlsson U and Jonsson BH. (2000) *Exs*: 241–259.
20. Semisotnov GV, Rodionova NA, Razgulyaev OI, Uversky VN, Gripas AF and Gilmanshin RI. (1991) *Biopolymers* **31**: 119–128.
21. Binford JS, Lindskog S and Wadso I. (1974) *Biochim. Biophys. Acta* **341**: 345–356.
22. Khalifah RG, Zhang F, Parr JS and Rowe ES. (1993) *Biochemistry* **32**: 3058–3066.
23. Stams T and Christianson DW. (2000) *Exs*: 159–174.
24. Coleman JE. (1975) *Annu. Rev. Pharmacol.* **15**: 221–242.
25. Maren TH and Sanyal G. (1983) *Annu. Rev. Pharmacol. Toxicol.* **23**: 439–459.
26. Supuran CT, Briganti F, Tilli S, Chegwiddden WR and Scozzafava A. (2001) *Bioorg. Med. Chem.* **9**: 703–714.
27. Matulis D, Salemme R and Todd M. (2004) in preparation.
28. Pantoliano MW, Petrella EC, Kwasnoski JD, Lobanov VS, Myslik J, Graf E, Carver T, Asel E, Springer BA, Lane P and Salemme FR. (2001) *J. Biomol. Screen.* **6**: 429–440.
29. Matulis D and Todd M. (2004) *Biochemistry* in preparation.
30. Todd MJ and Salemme FR. (2003) *Genetic Eng. News* **23**.
31. Butler JN and Cogley DR. (1998) *Ionic Equilibrium. Solubility and pH Calculations*, Wiley, New York.
32. Chakravarty S and Kannan KK. (1994) *J. Mol. Biol.* **243**: 298–309.
33. Liljas A, Hakansson K, Jonsson BH and Xue Y. (1994) *Eur. J. Biochem.* **219**: 1–10.
34. Krebs JF and Fierke CA. (1993) *J. Biol. Chem.* **268**: 948–954.
35. Myszka DG, Abdiche Y, Arisaka F, Byron O, Eisenstein E, Hensley P, Lombardo C, Schwarz FP, Thommsom J, Stafford W and Doyle ML. (2003) *J. Biomol. Tech.* **14**: 247–269.